The influence of temporal context on vision over multiple time scales

Kacie Lee[1] & Reuben Rideaux[1,2]

[1]School of Psychology, The University of Sydney, Camperdown, Australia
[2]Queensland Brain Institute, The University of Queensland, St Lucia, Australia
corresponding author: reuben.rideaux@sydney.edu.au

Conflict of interest statement: The authors declare no competing interests.

Acknowledgements: We thank Arnaldo Bisbal, Leon Zhong, and Cecelia Chenh for assistance with data collection. We also thank Dr William Harrison for their feedback on an earlier version of the manuscript. This work was supported by Australian Research Council (ARC) Discovery Early Career Researcher Awards awarded to RR (DE210100790) a National Health and Medical Research Council (NHMRC; Australia) Investigator Grant (2026318).

Keywords: vision, predictive coding, serial dependence, sequential dependencies, statistical learning, temporal effects, EEG, pupillometry.

ABSTRACT

Past sensory experiences influence perception of the present. Multiple research subfields have emerged to study this phenomenon at different temporal scales. These phenomena fall into three categories: the influence of immediately preceding sensory events (micro), expectations established by short sequences of events (meso), and regularities over long sequences of events (macro). In a single paradigm, we examined the influence of temporal context on perception at each scale. By integrating behavioural and pupillometry recordings with electroencephalographical recordings from a previous study, we identify two distinct mechanisms that operate across all scales. The first is moderated by attention and supports rapid motor responses to expected events. The second operates independently of task-demands and dampens the feedforward neural responses produced by expected events, leading to unexpected events eliciting earlier and more precise neural representations.

INTRODUCTION

The capacity to adapt to patterns in the environment supports biological function from sensory processing to motor action. The temporal context in which sensory events are embedded can be leveraged to more effectively process and respond to this information. For example, expert tennis players predict the trajectory of the ball from the movements of their opponent and use this information to prepare their return (1). Influential theories of normative brain function such as predictive coding posit that temporal context serves to improve representational fidelity and reduce neurometabolic expenditure (2–4).

Humans are sensitive to the temporal context of events across multiple time scales. At the shortest scale, each event influences processing of the next event (**Fig. 1a**, micro). For example, stimulus reproductions are biased towards previous stimuli. This phenomenon is referred to as *serial dependency* and has been demonstrated for a range of visual and auditory features (5–7). At intermediate scales, short sequences of events form patterns that uniquely influence responses to subsequent events (**Fig. 1a**, meso). For instance, events that satisfy regular patterns produce attenuated neural responses (*oddball effect*) (8) and are responded to more quickly and accurately than events that violate them (*sequential dependencies*) (9, 10). At longer time scales, the relative frequency of past events can alter how those in the present are processed (**Fig. 1a**, macro). These effects are often referred to as *statistical learning* and are thought to reflect adaptation to regularities in the environment (11, 12).

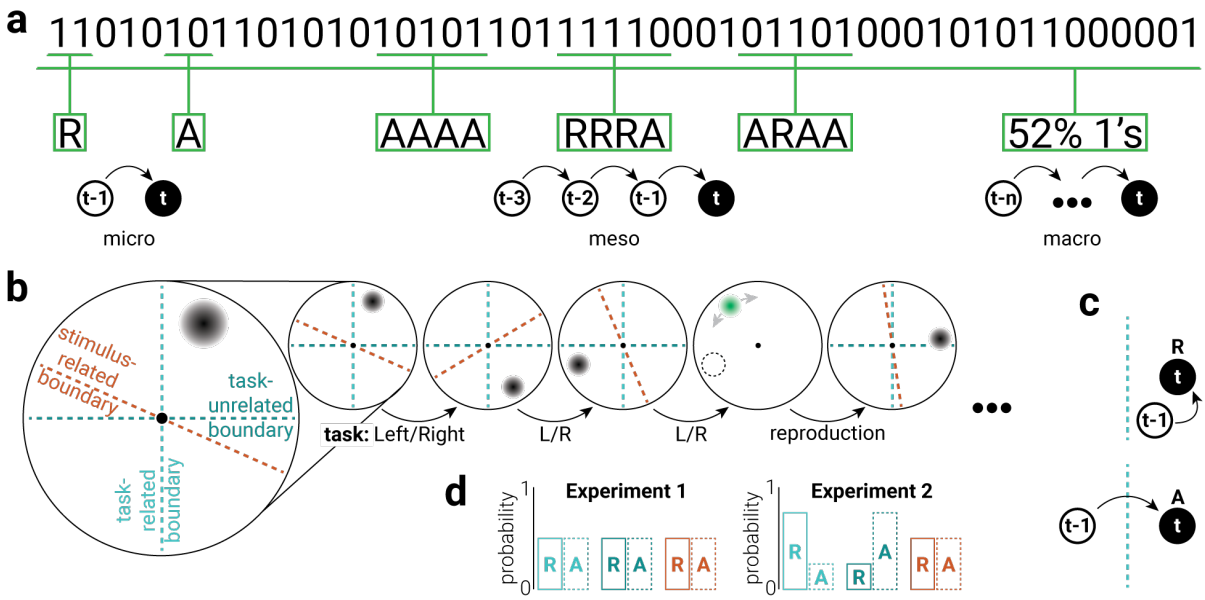

Figure 1. Multiple scales of temporal context. a) Illustration of three scales of temporal context in a binary time series. At the micro scale, events can either stay the same over time (repeat; R) or change (alternate; A). At the meso scale, short sequences of events (e.g., 5) form patterns that vary in their regularity (e.g., four repeats of the same event seems more regular than a mixture of repeats and alternations between events). At the macro scale, general trends regarding the relative frequency of different events are formed over longer time periods. **b**) To test the influence of temporal context on visual perception across different scales, participants were instructed to indicate the location of serially presented targets, which were randomly positioned on an imaginary circle centered on fixation. Participants performed a speeded binary judgement (e.g., left/right of fixation) on each trial and additionally reproduced the location of the target on 10% of trials. Trials were categorized as either (**c**, top) repeat (R) or (**c**, bottom) alternate (A) based on the location of the target relative to the previous target, according to three spatial reference planes: task-related (light cyan), task-unrelated (dark cyan), and stimulus-related (orange). **d**) In Experiment 1, the location of targets was uniformly sampled such that repeat and alternate trials were equally likely. In Experiment 2, the probability of repeat and alternate trials was biased across the task-related and unrelated planes.

Incoming sensory information is shaped by its temporal context across time scales that range many orders of magnitude. Previous work has developed a variety of experimental designs to isolate the influence of temporal context at each scale and examine its behavioural and neural consequences. This approach has propagated multiple fields of research and implicitly asserts qualitive differences, however, it limits comparison between temporal context at different scales. It is possible that temporal context serves perception differently at each time scale and is thus associated with unique adaptive influences on sensory processing. For example, perception may be best supported by one mechanism that promotes a set of outcomes from moment to moment and another mechanism that promotes a different set of outcomes in response to trends formed over long periods. Alternatively, a common rule may be

applied at all scales of temporal context, signalling a unifying adaptive mechanism. Predictive coding theory offers a normative framework with which to understand the influence of temporal context across scales, but contradictory evidence (3, 13–15) (i.e., sharpening or dampening of expected events) from distinct experimental paradigms has challenged this unification.

We designed a novel paradigm to investigate how temporal context shapes perception across multiple scales. We further used electroencephalography (EEG) and pupillometry recordings to characterize the neural mechanisms associated with these perceptual consequences. We identify two distinct mechanisms that operate across all scales. The first is moderated by attention and supports rapid motor responses to expected events. The second is independent of task-demands and dampens the feedforward neural responses to expected events, leading to unexpected events eliciting earlier and more precise neural representations. Together, these adaptive mechanisms explain a raft of temporal sensory phenomena, and provide evidence for a dampening account of predictive coding.

RESULTS

To measure changes in visual perception associated with different scales of temporal context, we tasked participants with indicating the location of serially presented visual stimuli (gaussian blobs randomly positioned at a fixed distance around a central fixation point). To assess response time and task accuracy, participants performed a speeded binary judgement (e.g., left or right of fixation) on each trial. On 10% of trials, participants additionally reproduced the location of the stimulus, providing a measure of recall precision. To test the influence of attention, trials were sorted according to two spatial reference planes, based on the location of the stimulus: task-related and task-unrelated (**Fig. 1b**). The task-related plane corresponded to participants' binary judgement (**Fig 1b**, light cyan vertical dashed line) and the task-unrelated plane was orthogonal to this (**Fig 1b**, dark cyan horizontal dashed line). For example, if a participant was tasked with performing a left-or-right-of-fixation judgement, then their task-related plane was the vertical boundary between the left and right side of fixation, while their task-unrelated plane was the horizontal boundary. The former (left-right) axis is relevant to their task while the latter (top-bottom) axis is orthogonal and task irrelevant. This orthogonality can be leveraged to analyze the same data twice (once according to the task-related plane and again according to the task-unrelated plane) in order to compare performance when the relative location of an event is either task relevant or irrelevant.

Micro-scale temporal context. At the shortest temporal scale, the speed with which events are responded to can be influenced by those that immediately precede them (16). We investigated the influence of the previous stimulus on the current stimulus by comparing responses between trials in which the previous stimulus was presented either on the same side (repeat) or the other side (alternate) of the reference plane (**Fig. 1c**, **2a**). Consistent with previous work (16), we found faster and more accurate responses to repeat stimuli along the task-related plane (speed: z_{75}=2.33, p=.020, r=.27; task accuracy: z_{72}=2.41, p=.016, r=.28; **Fig. 2b-c**, light cyan). However, in contrast, we found that repeat stimuli were recalled less precisely than alternate stimuli (z_{72}=3.74, p=2.00e^{-4}, r=.44; **Fig. 2d**, light cyan). For the task-unrelated plane, we found faster responses for repeat stimuli, but no difference in task accuracy, and marginally higher precision for alternate stimuli (speed: z_{75}=6.66, p=2.76e^{-11}, r=.77;

accuracy: z_{72}=0.92, p=.357, r=.11; precision: z_{76}=1.62, p=.105, r=.19; **Fig. 2b-d**, dark cyan).

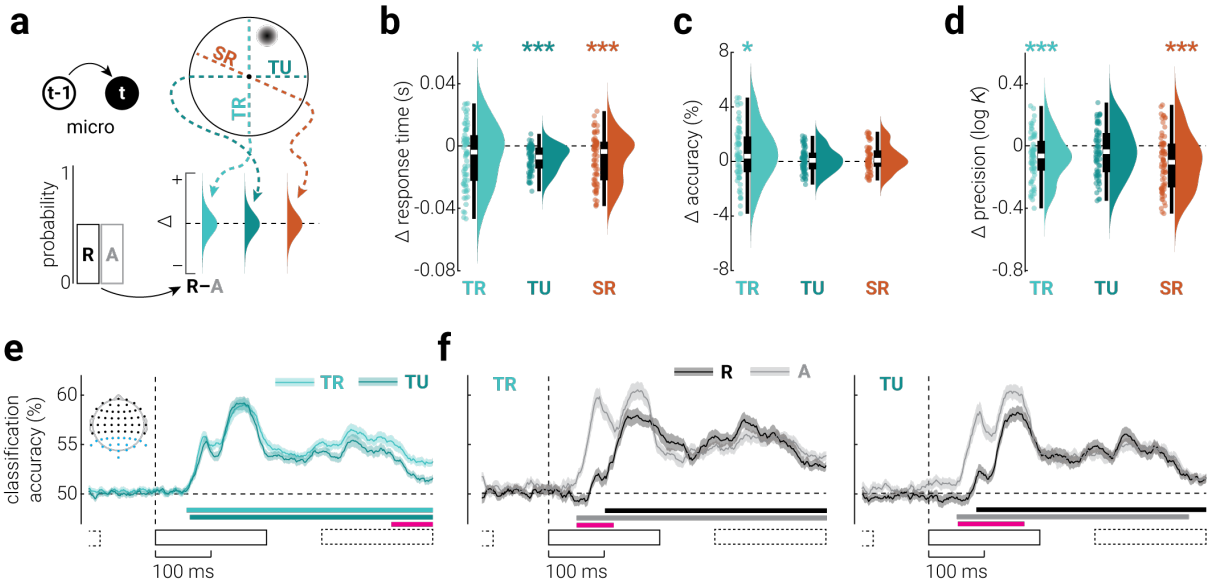

Figure 2. The influence of micro-scale temporal context on visual processing. a) Micro temporal context refers to the influence of the last event on the current event. We assessed its influence by comparing task performance for repeat and alternate presentations along task-related (light cyan), task-unrelated (dark cyan), and stimulus-related (orange) reference planes. **b-d**) The difference (repeat – alternate) in (**b**) response time, (**c**) task accuracy, and (**d**) precision for the three references planes. Asterisks indicate significant differences (*p<.05, **p<.01, ***p<.001). **e**) Classification accuracy of stimuli presented on different sides of task-related and unrelated planes, from re-analysis of previously published EEG data (17). **f**) Same as (**e**), but split into repeat and alternate stimuli, along (left) task-related and (right) unrelated planes. Inset in (**e**) shows the EEG sensors included in the analysis (blue dots). Black rectangles indicate the timing of stimulus presentations (solid: target stimulus, dashed: previous and subsequent stimuli). Shaded regions indicate ±SEM. Horizontal bars indicate cluster corrected periods of significance (cyan and greyscale: above chance classification accuracy, pink: difference).

While the difference in response time for repeat and alternate stimuli were of similar magnitude between task-related and unrelated planes (z_{71}=1.15, p=.249), the *variance* across participants was considerably higher in the former condition ($F_{1,140}$=46.26, p=2.76e^{-10}). The increased variability of response time differences across the task-related plane likely reflects individual differences in attention and prioritization of responding either quickly or accurately. On each trial, the correct response (e.g., left or right) was equally probable. So, to perform the task accurately, participants were motivated to respond without bias, i.e., without being influenced by the previous stimulus. We would expect this to reduce the difference in response time for repeat and alternate stimuli across the task-related plane, but not the task-unrelated plane. However, task-relatedness may amplify the bias towards making

faster responses for repeat stimuli, by increasing attention to the identity of stimuli as either repeats or alternations (17). These two opposing forces vary with task engagement and strategy and thus would be expected produce increased variability across the task-related plane. Unlike response time, we would not expect task accuracy to be modulated by task-unrelated micro temporal context, as the tasks were orthogonal. That is, while a repeat along the task-unrelated plane may increase the speed with which an (in/correct) response is made along the task-related plane, it would not be expected to change the type of response (e.g., left or right). Precision differences were similar between task-related and unrelated planes, both in terms of magnitude (z_{70}=1.77, p=.076) and variability ($F_{1,138}$=0.66, p=.417), suggesting that modulation of representational fidelity may be operationalized by a distinct mechanism to that which modifies response speed, and is not moderated by attention.

These results could be interpreted as a general expectation that sensory events, e.g., the image of an object on the retina, are more likely to stay the same than to change (7). Through this lens, these findings would indicate that micro temporal context leads to faster and more accurate responses to expected events, but more precise encoding of unexpected events. As we will show, these two outcomes resonate across all levels of temporal context and point to two distinct mechanisms that unify the influence of past experiences on perception.

To test for neural correlates of micro temporal context, we re-analyzed a previously published EEG dataset in which human participants viewed visual (arc) stimuli presented at random angles around fixation, while monitoring for targets (stimuli presented at a specific location) (17). We used multivariate linear-discriminant analysis to classify the location of stimuli according to task-related (< or > |90°| from target angle) and unrelated planes (orthogonal to task-related plane), from parietal and occipital sensors (**Supplementary Fig. 1a**). We found that classification accuracy was higher across the task-related plane (**Fig. 2e**).

In separately assessing classification accuracy for repeat and alternate stimuli, we found temporal dependencies that were due to low frequency signals, unrelated to stimulus properties, as evidenced by their presence in results produced from data with shuffled labels (see **Supplementary Fig. 2** for a full description of the temporal

dependencies). We removed these general temporal dependencies by subtracting the bias in the shuffled data from the original classification accuracy. For both task-related and unrelated planes, we found that classification accuracy was higher for alternate stimuli from ~60-160 ms (i.e., the first moments of reliable stimulus decoding) and that alternate stimuli could be reliably classified ~20 ms earlier than repeat stimuli (**Fig. 2f**). The difference in classification accuracy between repeat and alternate stimuli was the same for task-related and unrelated conditions. This neural phenomenon may explain the increased behavioural recall precision observed for alternate stimuli. The timing and task-independence of this phenomenon points to a passive, massively parallel, mechanism that operates on feedforward sensory signals, by supressing responses to repeat stimuli.

Another phenomenon associated with micro temporal context is *serial dependence*, i.e., reproductions of events from memory are biased towards the events that immediately preceded them (5, 7). To assess serial dependence in the behavioural data, we began by comparing behavioural performance across a third, stimulus-related, plane (**Fig 2a**, orange); whereas task planes were constant, the stimulus-related plane was defined by the location of the stimulus on the previous trial, and thus varied from trial to trial. That is, on each trial, the target is considered a repeat if it changes location by <|90°| relative to its location on the previous trial, and an alternate if it changes by >|90°|. We found a similar pattern of results as those for task-related and unrelated planes: responses were faster for stimuli that repeated (z_{77}=3.73, p=2.00e^{-4}, r=.43; **Fig. 2b**, orange) but more precise for those that alternated (z_{76}=4.51, p=6.34e^{-6}, r=.52; **Fig. 2d**, orange). The latter result is inconsistent with previous work on serial dependence, which has reported more precise judgements when subsequently presented stimuli are similar (18).

To further investigate the influence of micro temporal context, we computed task performance as a function of the angular distance from the previous stimulus (*Δ location*). We calculated the bias of reproduction responses as a function of Δ location and found the archetypal pattern of attractive biases associated with serial dependence (**Fig. 3a**). Consistent with our previous binary analysis, and with previous work (19), we also found that responses were faster and more accurate when Δ location was small (**Fig. 3b**, **c**). We further found that the precision of responses

peaked at both large and small Δ locations, with the worst precision for stimuli with around ±60° Δ location (**Fig. 3d**). The peak in precision for large Δ locations is consistent with alternate events being encoded more precisely, while the peak for small offsets may be explained the attractive bias towards the previous target.

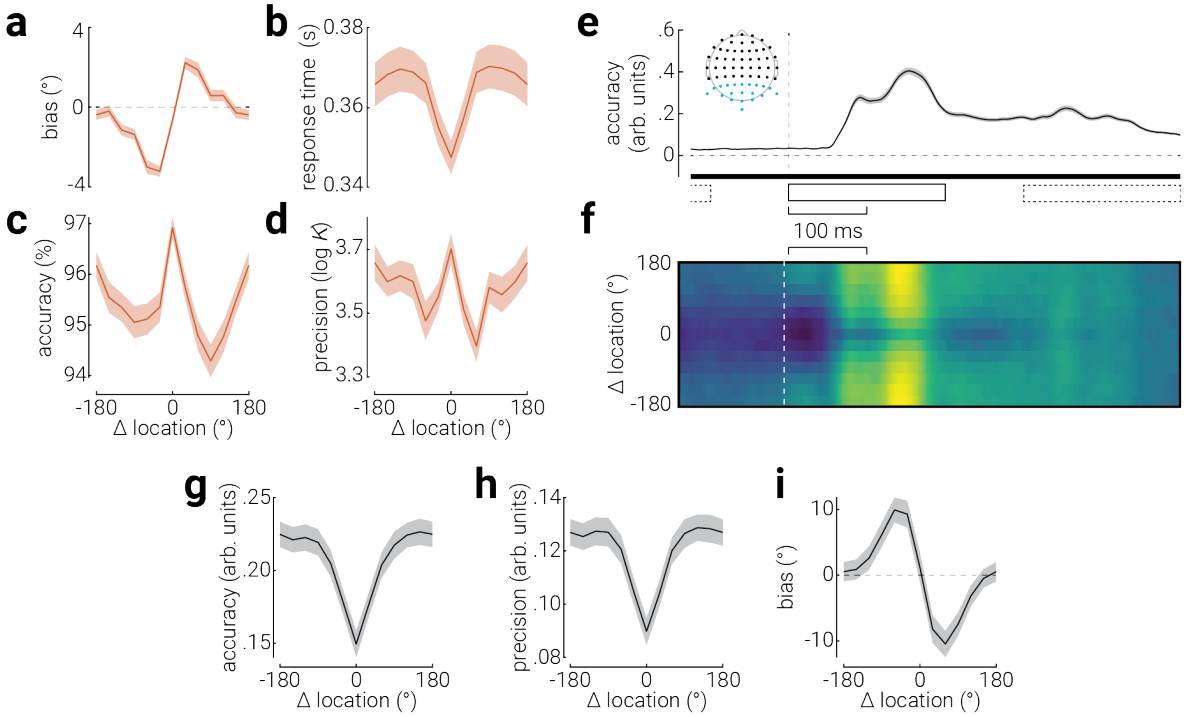

Figure 3. The influence of serial dependence on visual processing. Serial dependence is associated with sensory stimuli being reported as more similar to previous stimuli and is typically assessed by measuring the perception of stimuli as a function of their distance to previous stimuli (Δ location). **a**) Location reproduction bias, (**b**) binary task response time and (**c**) accuracy, and (**d**) reproduction precision as a function of distance from the previous stimulus. **e**) Decoding accuracy for stimulus location, from re-analysis of previously published EEG data (17). Inset shows the EEG sensors included in the analysis (blue dots), and black rectangles indicate the timing of stimulus presentations (solid: target stimulus, dashed: previous and subsequent stimuli). **f**) Decoding accuracy for location, as a function of time and Δ location. Bright colours indicate higher decoding accuracy; absolute accuracy values can be inferred from (**e**). **g-i**) Average location decoding (**g**) accuracy, (**h**) precision, and (**h**) bias from 50 – 500 ms following stimulus onset. Horizontal bar in (**e**) indicates cluster corrected periods of significance; note, all time points were significantly above chance due to temporal smear introduced by high-pass filtering (see **Supplementary Figure 3** for full details). Note, the temporal abscissa is aligned across (**e** & **f**). Shaded regions indicate ±SEM.

To further investigate the influence of serial dependence, we applied inverted encoding modelling to the EEG recordings to decode the angular location of stimuli. We found that decoding accuracy sharply increased from ~60 ms following stimulus onset (**Fig. 3e**). Note, to remove the influence of general temporal dependencies, we applied a 0.7 Hz high-pass filter to the data, which temporally smeared the stimulus-related information, resulting in above-chance decoding accuracy prior to stimulus

presentation (for full details, see **Supplementary Figure 3**). To understand how serial dependence influences the representation of these features, we inspected decoding accuracy as a function of both time and Δ location (**Fig. 3f**). We found that decoding accuracy varied depending not only as a function of time, but also as a function of Δ location. To characterise the latter relationship, we calculated the average decoding accuracy from 50 ms until the end of the epoch (500 ms), as a function of Δ location (**Fig. 3g**). This revealed higher accuracy for targets with larger Δ location. We found a similar pattern of results for decoding precision (**Fig. 3h**). These results are consistent with the micro temporal context (behavioural) results, showing that targets that alternated were recalled more precisely. Lastly, we calculated the decoding bias as a function of Δ location and found a clear repulsive bias away from the previous stimulus (**Fig. 3i**). While this result is inconsistent with the attractive behavioural bias, it is consistent with recent studies of serial dependence suggesting an initial pattern of repulsion followed by an attractive bias during the response period (20–22).

Meso-scale temporal context. The influence of recent events can accrue over time, producing unique changes in behavioural responses associated with short sequences of stimuli (**Fig. 4a**). Higher-order sequential dependences are an example of how stimuli (at least) as far back as five events in the past can shape the speed and task accuracy of responses to the current stimulus (9, 10); however, note that these effects have been observed for more than five events (23). For five binary events (e.g., left or right), there are 16 possible sequences of repeat and alternate stimuli. Typically, sequential dependencies are assessed by computing the average response time and/or task accuracy for stimuli, binned according to which of these 16 sequences reflects their recent history. The differences observed between sequences have been interpreted as indicative of the expectation of the current stimulus, based on previous events (9).

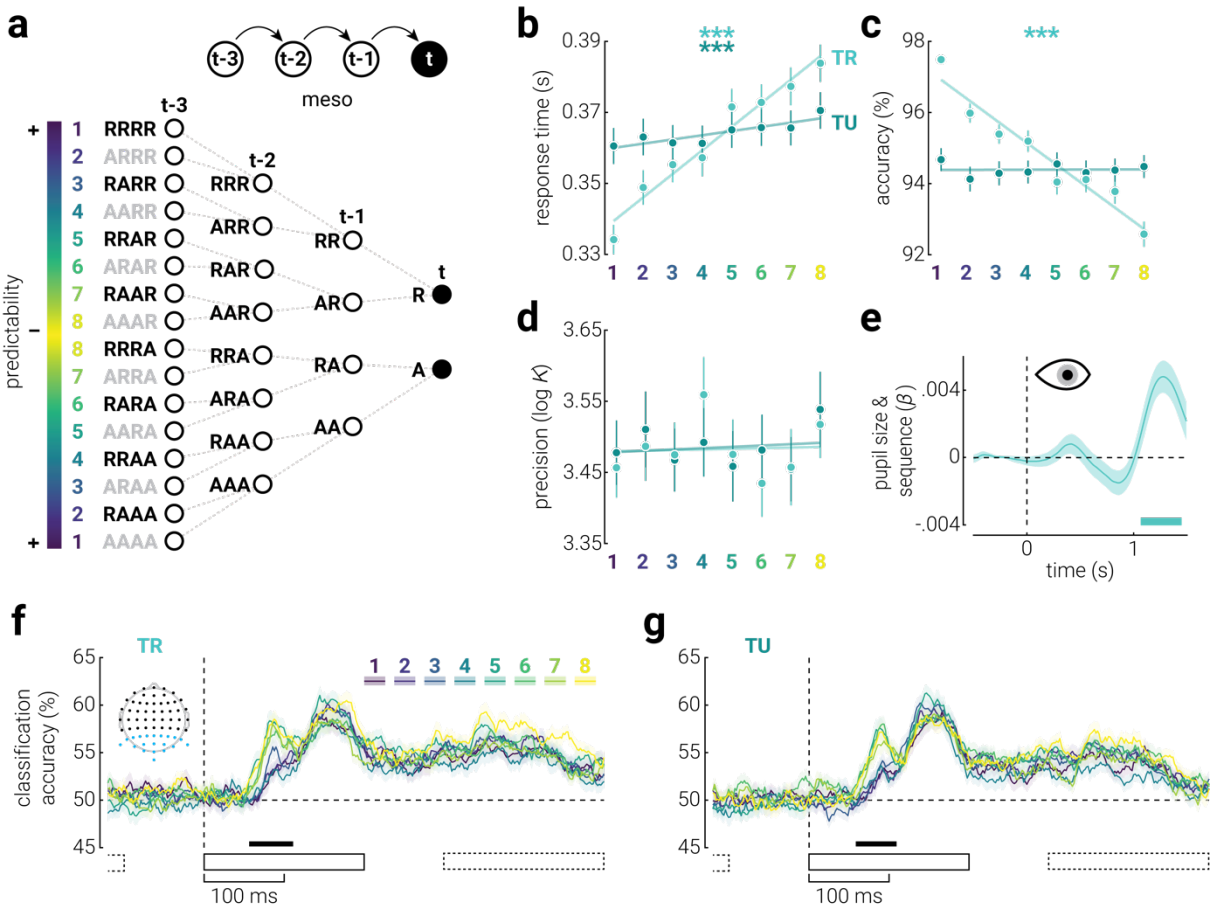

Figure 4. The influence of meso-scale temporal context on visual processing. a) Illustration of all 16 possible sequences of repeat and alternate events for a series of five binary events. Sequences are arranged symmetrically such that those for which the final event is thought to be most expected are at the top and bottom and those for which the final event is least expected are in the middle. To control for differences between repeat and alternate events, we combined symmetric pairs, resulting in a total of eight sequences. **b**) Response time, (**c**) task accuracy, and (**d**) precision as a function of sequence, across task-related and unrelated reference planes. Note, lower numbers on the abscissa are associated with sequences in which the final target stimulus is more expected. Asterisks indicate significant main effects of sequence (***p<.001). Error bars indicate ±SEM; semi-transparent lines indicate linear fits to the data. **e**) The correlation between pupil size and sequence as a function of time. Note, we did not analyze pupillometry data for micro temporal context due the confounding effect of differential foveal luminance between repeat and alternate stimuli. **f**) Classification accuracy of stimuli presented on different sides of task-related planes as a function of time, for each of the eight sequences, from re-analysis of previously published EEG data (17). **g**) Same as (**f**), but for the task-unrelated plane. Inset in (**f**) shows the EEG sensors included in the analysis (blue dots). Black rectangles indicate the timing of stimulus presentations (solid: target stimulus, dashed: previous and subsequent stimuli). Shaded regions indicate ±SEM. Horizontal bars indicate cluster corrected periods of significant relationships between (**e**) pupil size or (**f, g**) classification accuracy and sequence order.

We tested the influence of higher-order sequential dependencies on response time, task accuracy, and recall precision, across task-related and unrelated reference planes. However, we first isolated the influence of meso temporal context from that of micro context (i.e., difference in performance between repeat and alternate stimuli), by binning responses into eight sequences formed by combining the symmetric

partners in the 16-sequence array (e.g., RRRR with AAAA, RRRA with AAAR, etc.). Thus, the frequency of repeat and alternate stimuli was equal across the eight sequences and any differences observed in performance are unlikely to be due to differential responses to these events. We found that responses were faster for sequences with expected targets across both reference planes (task-related: $\chi^2_{7,469}$=375.86, p=3.56e^{-77}, W=.84; task-unrelated: $\chi^2_{7,483}$=110.94, p=5.85e^{-21}, W=.26; **Fig. 4b**). Responses were also more accurate for expected targets across the task-related plane ($\chi^2_{7,399}$=208.37, p=2.03e^{-41}, W=.44; **Fig. 4c**). By contrast, we found no such clear relationship between precision and expectancy (both p>.05; **Fig. 4d**).

We found that micro temporal context influenced recall precision, whereas we did not detect significant modulation of precision for meso context. This may be because meso temporal effects reflect motor priming and do not precipitate visual predictions. When predictions are violated, the pupils dilate in what has been interpreted as an arousal response (24, 25). We found that participants' pupils dilated more in response to unexpected sequences (**Fig. 4d**), indicating that meso temporal context establishes sensory predictions. Another possible explanation why we did not detect an effect on recall precision is that we lacked statistical power. The micro analyses split data between two conditions (repeat and alternate), whereas in the meso analysis, data is split between eight (sequences). Indeed, in our second experiment, we reproduced the response time and task accuracy effects of meso temporal context and further found that unexpected sequences were recalled more precisely (**Supplementary Fig. 4**).

To further test whether meso temporal context effects were qualitatively different from those at the micro scale, we separated the EEG classification accuracies (**Fig. 2e**) into the eight sequence categories and corrected for shuffled accuracy (**Supplementary Fig. 5**). We found a strikingly similar pattern of results to those observed at the micro scale: there was increased classification accuracy for unexpected sequences from ~60-100 ms along both task-related and unrelated reference planes (**Fig. 4h**, **g**). This finding provides further evidence of a passive mechanism that suppresses feedforward sensory activity elicited by expected stimuli and leads to more precise recall of those that are unexpected. That the effect was

reproduced when repeat and alternate stimuli were matched also shows that it cannot be explained by sensory adaptation (26).

Macro-scale temporal context. Events within micro and meso temporal contexts occur within the limits of short-term memory. Most events that occur further into the past cannot be recalled; yet, they continue to influence perception (11, 12). To test the influence of macro temporal context on perception, we ran a second experiment in which the probability of stimulus presentation was biased towards repeats or alternates along task-related and unrelated reference planes (**Fig. 1d**, Experiment 2). The biases were counterbalanced across participants such that we could compare performance between relatively frequent (expected) and infrequent (unexpected) events, while controlling for differences between repeat and alternate stimuli (**Fig. 5a**). Consistent with micro and meso scale effects, we found that expected events were responded to faster and more accurately, while unexpected events were reproduced more precisely, across both task-related (speed: z_{78}=7.67, p=1.68e^{-14}, r=.87; task accuracy: z_{73}=7.42, p=1.13e^{-13}, r=.87; precision: z_{79}=3.26, p=.001, r=.37) and unrelated planes (speed: z_{71}=6.69, p=2.19e^{-11}, r=.79; task accuracy: z_{78}=6.76, p=1.32e^{-11}, r=.77; precision: z_{75}=2.72, p=.007, r=.31; **Fig. 5b-d**). This effect was larger along the task-related plane for response time and task accuracy, but not precision (speed: z_{71}=7.24, p=4.42e^{-13}, r=.86; task accuracy: z_{78}=7.27, p=3.52e^{-13}, r=.82; precision: z_{75}=0.93, p=.350, r=.11). Pupillometry analysis further revealed that participants' pupils dilated more in response to unexpected stimuli ~1 s after stimulus onset (**Fig. 5e**).

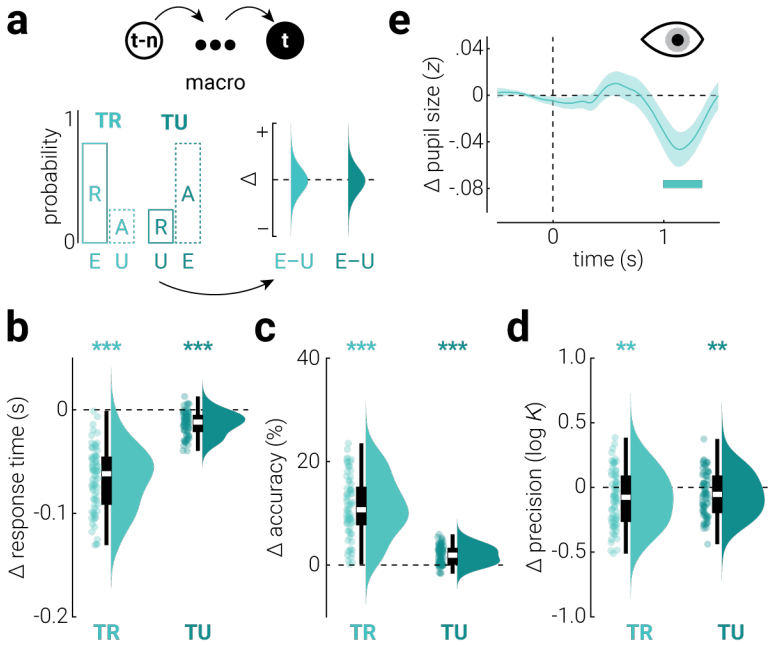

Figure 5. The influence of macro temporal context on visual processing. a) Repeat (R) and alternate (A) stimuli were presented with unequal probabilities (counterbalanced across participants) along task-related and unrelated reference planes. The difference in performance between relatively frequent (expected; E) and infrequent (unexpected; U) stimuli was calculated to assess the influence of macro temporal context on visual processing. **b-d**) The difference (expected – unexpected) in (**b**) response time, (**c**) task accuracy, and (**d**) reproduction precision between expected and unexpected stimuli, along task-related (TR) and unrelated (TU) planes. Note that we observed task accuracy differences associated with macro temporal context across the task-unrelated plane. In the micro and meso analyses, the expected outcome along the task-unrelated plane was never in conflict with that in the task-related plane. For example, if a stimulus is expected on the same (right) side of the display (repeat; task-related plane), then regardless of whether the stimulus appeared above or below fixation, there was a quadrant of the display that would satisfy both the task-related and unrelated expectations (bottom- or top-right). This is because the expectation was either for repeat stimuli (micro) or balanced between repeat and alternate stimuli (meso). By contrast, in the macro condition, where stimuli could be expected to alternate, this produced trials on which the task-related and unrelated expectations conflicted, such that there was no location that could satisfy both. Accuracy along the task-unrelated plane was reduced in these instances where there was conflict. Asterisks indicate significant differences (**p<.01, ***p<.001). **e**) The difference (expected – unexpected) in pupil size as a function of time from stimulus presentation, along the task-related (TR) plane. Shaded region indicates ±SEM and the horizontal bar indicates a cluster corrected period of significant difference.

In line with previous work, stimuli in our experiment were displayed until participants responded. To test how variable presentation duration influenced the results, we ran a third experiment that was the same as the second, except with a fixed stimulus duration (200 ms). Experiment 3 replicated both the behavioural and pupillometry results from Experiment 2 (**Supplementary Fig. 6**), indicating that the effects observed were not related to variable stimulus duration.

DISCUSSION

Evidence from multiple, separate, fields of research show that humans are sensitive to the temporal context in which sensory stimuli are embedded across a broad range of time scales. Here we used a novel experimental paradigm to characterise and compare how past sensory events occurring at different temporal scales shape perception of the present. By combining behavioural, neuroimaging, and physiological approaches to assess the influence of temporal context at the micro, meso, and macro scale, we identified new properties of these phenomena in isolation and further revealed two distinct adaptive mechanisms that unify them.

Micro-scale temporal context. At the micro scale, stimuli were responded to faster and more accurately when preceded by those that were similar, but recalled more precisely when preceded by those that were different. This may reflect a general expectation that objects in the environment are more likely to stay the same than to change (7). Under this interpretation, expected events are rapidly responded to while unexpected events are precisely encoded. As will be discussed shortly, this interpretation resonates with the influence of temporal context at longer scales.

Analysis of EEG recordings showed that during the initial stage of stimulus processing in the cortex (60 ms after onset), alternating stimuli were represented both (20 ms) earlier and more robustly than those that repeat. This finding provides a neural correlate of the improved recall precision for these stimuli and, consistent with recent psychophysical work (27), suggests that unexpected (alternating) events are prioritized in terms of both encoding fidelity and processing speed. Given that unexpected stimuli were responded to more slowly than expected stimuli, despite benefitting from sensory processing priority, this may indicate that the latter is supported by anticipatory motoric activity (28).

Effects on binary judgements associated with micro temporal context, such as those described above, have been referred to as first-order sequential dependencies (16). By contrast, those associated with continuous report tasks are typically referred to as serial dependence (5, 7). We examined behavioural responses for continuous effects and found the stereotypical pattern of response biases associated with serial dependence, i.e., attraction towards the preceding stimulus.

Our corresponding EEG analyses revealed better decoding accuracy and precision for stimuli preceded by those that were different and a bias away from the previous stimulus. These results are consistent with finding that alternating stimuli are recalled more precisely. Further, while the repulsive pattern of biases is inconsistent with the observed behavioural attractive biases, it is consistent with recent work on serial dependence indicating an initial period of repulsion, followed by an attractive bias during the response period (20–22). These findings indicate that serial dependence and first-order sequential dependencies can be explained by the same underlying principle. Behavioural and neural recordings show a predisposition for expected outcomes, which manifest as faster, biased, behavioural responses. By contrast, unexpected outcomes are encoded earlier and more precisely, leading to increased recall fidelity for these events.

Meso-scale temporal context. At the meso scale, consistent with previous work (9, 10), we found that short sequences of stimuli were responded to faster and more accurately when they were expected. Extending these findings, and matching the influence of micro-scale temporal context, we also found that responses were more precise for unexpected sequences (in Experiment 2, and non-significantly in Experiment 1). Pupillometry analyses confirmed that participants were surprised by stimuli that were categorized as unexpected, and EEG analyses revealed a strikingly similar pattern of results as was found at the micro scale. In particular, unexpected stimuli were encoded earlier and more robustly. The similarity between the influence at the micro and meso scale is particularly remarkable given that the influence of micro temporal context was controlled for in the meso-scale analyses.

Theoretical and empirical work has implicated both motor and sensory priming in the modulation of response time and accuracy associated with higher-order sequential dependencies (28–30). Decoupling the motoric component of experimental designs used to probe the phenomenon has been an obstacle to assessing how sensory processing is influenced by meso-scale temporal context. In the EEG experiment that was re-analyzed here, participants viewed serially presented stimuli and were tasked with reporting the number of targets after 30 presentations. Thus, there were no motor actions generated during the recording period used to perform the analysis and our results can only be attributed to differences in visual

processing between sequences. Indeed, the timing of the improved encoding of unexpected sequences, like that for micro temporal context, can only be accounted for by a mechanism that prioritizes the encoding speed and fidelity of stimuli during the initial feedforward cascade of sensory processing.

Macro temporal context. Results from our second experiment, in which biases in the probability of repeat and alternate stimuli were introduced, showed that responses are faster and more accurate for expected stimuli, and that recall precision is better for unexpected stimuli. Pupillometry analysis confirmed that participants were surprised by unexpected stimuli. We replicated these results in a third experiment, demonstrating that the same outcome for stimuli of fixed duration. These findings parallel those observed at the micro and meso scales and point to two canonical adaptive mechanisms that operate across a wide range of temporal contexts to support a common sensory outcome.

The role of attention. At each scale, we found that attention (operationalized through task-relatedness) amplified the influence of temporal context for response time and task accuracy, but not precision. These findings suggest that perception and behaviour are modulated by expectation through two distinct mechanisms. One mechanism is sensitive to top-down goals (attention) and supports rapid responses to expected stimuli, while the other mechanism automatically detects mismatches between expected and actual outcomes and prioritizes the encoding speed and fidelity of unexpected stimuli. In line with this, some studies have reported interactions between attention and predictive mechanisms (31, 32), while others have shown that oddball event-related potentials can be detected in coma patients (33).

Consistent with previous work (17), we found that the influence of attention on the neural representation only emerged after ~200 ms. By contrast, we found that effects of expectation, for both micro- and meso-scale temporal context, were present during the earliest moments of cortical sensory processing, i.e., during the feedforward cascade. These findings suggest that predictive mechanisms are operational during feedforward processing, while attention modulates sensory processing at a later stage.

447 ***Predictive coding.*** Predictive coding theories argue that *prediction errors* are
448 generated when bottom-up sensory inputs deviate from top-down expectations (3).
449 There is broad consensus that prediction errors are associated with increased neural
450 activation (13, 34–38), which is typically observed during the initial processing cascade
451 in sensory cortices associated with the unexpected stimulus (39, 40), but has also
452 been reported in subcortical regions (24). By contrast, whether this modulation of
453 neural activation results from 'dampening' or 'sharpening' of the neurons tuned to
454 expected features remains highly contested (3, 13–15, 41). Whether through
455 increased selectively (sharpening) or reduced sensitivity (dampening), both accounts
456 predict attenuated activation in response to expected events. However, according to
457 the sharpening model, expected events are represented more precisely, while the
458 dampening model posits the opposite, i.e., unexpected events are more precisely
459 represented. At every scale of temporal context and across behavioural and neural
460 recordings, we consistently found that unexpected events were encoded more
461 precisely than expected events. These findings provide compelling evidence that
462 predictive mechanisms reduce the sensitivity of neurons tuned to expected features,
463 likely in order to reduce metabolic energy expenditure (3), rather than increasing their
464 selectively.

465 The expectation of stimuli shaped their neural representation in a robust and
466 striking manner. In particular, the peak in classification accuracy from 50-150 ms
467 following stimulus onset, which represents the initial stage of (feedforward) cortical
468 representation, was almost entirely accounted for by stimulus expectation such that
469 expected stimuli were only minimally represented during this period. This modulation
470 cannot be attributed to adaptation, as we found the same result at the meso scale,
471 where the change in location between subsequent stimuli was matched between
472 conditions. Further, we found an attractive bias during this period, as opposed to the
473 repulsive bias associated with adaptation. There was relatively weak evidence for a
474 difference between the neural representation of expected and unexpected stimuli
475 following this initial peak. Given that unexpected stimuli were recalled more precisely
476 in the behavioural task, this provides further support to the notion that recall of these
477 stimuli primarily reflects neural activity during this initial stage of sensory processing;
478 however, more work is needed to understand how this relationship changes with

increasing stimulus complexity. These findings provide empirical evidence that predictive mechanisms operate to reduce the feedforward sensory activity associated with expected stimuli in a manner that reduces their representational fidelity (i.e., dampening/cancellation).

Prioritizing the speed and fidelity with which unexpected events are encoded likely serves to rapidly and precisely update internal predictive models when there is a mismatch between predictions and incoming sensory information. By contrast, expected events may benefit from anticipatory motoric activation, which facilitates rapid behavioural responses, and do not require encoding prioritization.

Limitations and future directions. One potential limitation of the current study is the categorization of temporal scales according to events, independent of the influence of event duration. While this simplification of time supports comparison between different phenomena associated with each scale (e.g., serial dependence, sequential dependencies, statistical learning), future work could investigate the role of duration to provide a more comprehensive understanding of the mechanisms identified in the current study. Related to this, while the temporal scales applied here conveniently categorized known sensory phenomena, and partially correspond to iconic-, short-, and long-term memory, there are alternative ways of delineating time. For example, temporal scales could be defined simply as short- and long-term (42). However, this could obscure meaningful differences between phenomena associated with sensory persistence and short-term memory, or qualitative differences in the way that short-sequences of events are processed.

Another limitation of the current study is that the EEG recordings were collected in a separate experiment to the behavioural and pupillometry data. The stimuli and task were similar between experiments, but not identical. For example, the EEG experiment employed coloured arc stimuli presented at a constant rate of ~3.3 Hz and participants were tasked with counting the number of stimuli presented at a target location. By contrast, in the behavioural experiment, participants viewed white blobs presented at an average rate of ~2.8 Hz and performed a binary spatial task coupled with an infrequent reproduction task. An advantage of this was that the sensory responses to stimuli in the EEG recordings were not conflated with motor responses;

however, future work combining these measures in the same experiment would serve as a validation for the current results.

Conclusion. Past sensory information shapes perception of the present. Multiple research areas have emerged to investigate the isolated influence of temporal context at different scales. In a single experimental paradigm, we compared the influence of past stimuli at micro, meso, and macro temporal scales, and found two common rules that characterized the relationship between the past and present across all ranges. While the neural mechanisms that implement the influence of temporal context across different scales may vary (e.g., tonic inhibition/excitation, synaptic weight), they appear to promote a two unifying outcomes: 1) rapid motor responses to expected events, and 2) prioritized encoding speed and fidelity of unexpected events.

METHODS

Participants. Eighty neurotypical human adults participated in Experiments 1 and 2 (mean±standard deviation age, Experiment 1: 20.9±2.9 years, 14 males, 65 females, 1 non-binary, Experiment 2: 21.0±5.8 years, 18 males, 62 females), and 40 neurotypical human adults participated in Experiment 3 (24.7±8.3 years, 10 males, 30 females. The data of one participant was omitted from Experiment 1 because they were unable to complete the experiment. Sample size was informed by previous studies using similar psychophysical methods (27). Participants were recruited from The University of Sydney and had normal or corrected-to-normal vision (assessed using a standard Snellen eye chart). All participants were naïve to the aims of the experiment and gave informed written consent. The experiment was approved by The University of Sydney Human Research Ethics Committee.

Apparatus. The experiment was conducted in a dark acoustically shielded room. The stimuli were presented on a 41.5-inch ASUS ROG Swift OLED monitor with 3840 x 2160 resolution and a refresh rate of 120 Hz. Viewing distance was maintained at 1 m using a chin and head rest. Stimuli were generated in MATLAB v2020a (The MathWorks, Inc., Matick, MA) using Psychophysics Toolbox(43, 44) v3.0.18.13 (see http://psychtoolbox.org/). Gaze direction and pupil diameter were recorded monocularly (right eye) at 1 kHz using an EyeLink 1000 (SR Research Ltd., Ontario, Canada).

Stimuli, task, and procedure. The stimuli comprised white Gaussian blobs (standard deviation=0.3°, contrast=0.5) positioned 4° of visual angle from fixation (location randomly selected between 0-360°) on a black background. A centrally positioned white fixation dot (radius=0.25°) was presented to reduce eye movements. Stimuli were presented until the participant responded. Half the participants were instructed to use the “z” and “/” keys to indicate whether the stimulus appeared on the left or right of fixation, and the other half used the “b” and “t” keys to indicate whether it appeared above or below fixation; the keys were selected to map the relative positions on the keyboard to the orientation of the task. Participants performed 15 to 20 blocks of 100 trials (~90 min), receiving feedback on their response time and task accuracy at the end of each block. On 10% of randomly selected trials, after participants responded,

553 the target blob was replaced by a green blob at a random location (same size as target
554 blob), and participants were instructed to use the response keys to rotate the location
555 of the green blob around to the location of the previous target blob and press the
556 "spacebar" key to confirm their response.

557 Experiment 2 was the same as Experiment 1, except that biases were
558 introduced to the location of the target blob. In particular, sequentially presented target
559 stimuli were more likely to be presented on the same side (75%; repeat) than on the
560 other side (25%; alternate), or vice versa, along each of the task reference planes
561 (left/right and above/below). Thus, a 2 (task reference plane) × 2 (left/right bias) × 2
562 (above/below bias) design was used and the eight conditions were counterbalanced
563 across participants. On each trial, based on the location of the target on the previous
564 trial and the unique bias condition, the quadrant of the next target was probabilistically
565 determined and then the location was randomly selected within the quadrant. Critically,
566 the biases manipulated the probability of repeat and alternate stimuli, not the spatial
567 location (e.g., left or right). Experiment 3 was the same as Experiment 2, but stimuli
568 were presented for a fixed duration (0.2 s). This duration was selected because it was
569 below the normal range of response times and was intended to allow the stimulus to
570 be presented for the full duration before participants responded.

571 ***Eye tracking.*** Pupil size recordings were epoched to between -0.5 to 1.5 s around
572 target stimulus presentation. Pupillometry data were preprocessed by removing blinks
573 (0.1 s buffer window), removing outliers (median absolute deviation>2.5), interpolated,
574 bandpass filtered with a first-order Butterworth filter (highpass=15.6 Hz, lowpass=500
575 Hz), *z*-scored, baselined to the 0.5 s period before stimulus presentation, and
576 downsampled to 125 Hz, respectively. Due to hardware issues, pupil data were not
577 collected from one participant in Experiment 1, two in Experiment 2, and three in
578 Experiment 3.

579 ***Behavioural analyses.*** Trials were grouped according to whether stimuli repeated
580 (the previous stimulus was presented on the same side) or alternated (the previous
581 stimulus was presented on the opposite side) according to three reference planes:
582 task-related, task-unrelated, and stimulus-related. The task-related plane mapped
583 onto the participants' task condition (left-right or above-below) and the task-unrelated
584 plane was orthogonal to the task-related plane. For example, if a participant was

assigned the left-right task condition, the task-related plane was defined by the vertical meridian and the task-unrelated plane was defined by the horizontal meridian. The stimulus-related plane was defined by the line bisecting the fixation point at an angle orthogonal to the stimulus location on the previous trial, and thus changed over time.

For micro analyses, the difference in responses to repeat and alternate stimuli was compared. For meso analyses, trials were further sorted into eight pairs of unique sequences, based on the (repeat/alternate) identity of the previous five trials (**Fig. 4a**). For macro analyses in Experiment 2 and 3, repeat and alternate trials were grouped according whether they were expected (75% probability) or unexpected (25% probability), based on participants' experimental condition. For all analyses, sequences that were disrupted by a reproduction task or block advancement were omitted. For each participant, after removal of trials where response time exceeded 2 s, median response times and average task accuracy were calculated.

From the reproduction task, we sought to estimate participant's recall precision. It is likely that on some trials participants failed to encode the target and were forced to make a response guess. To isolate the recall precision from guess responses, we used mixture modelling to estimate the precision and guess rate of reproduction responses, based on the concentration (κ) and height of von Mises and uniform distributions, respectively (45). The κ parameter of the von Mises distribution reflects its width, which indicates the clustering of responses around a common location. For the serial dependency analysis, we calculated bias and precision by binning reproduction responses according to the angular offset between the current and previous target and then performing mixture modelling to estimate the mean (bias) and κ (precision) parameters of the von Mises distribution. Precision values were positively skewed across participants, so a logarithmic transformation was applied to normalize their distribution ($\log_{10} \kappa$). For serial dependence analyses, the location (μ) of the von Mises distribution was used to estimate response bias.

EEG. EEG data from a previously published dataset were re-analyzed (17). The stimuli comprised coloured arcs (inner ring, 0.25°; outer ring, 4.25°) extending 45° polar angle on a mid-grey background. Trials consisted of 30 arc stimuli (location and colour randomly selected between 0-360°) presented for 0.2 s each, separated by a blank 0.1 s inter-stimulus-interval. Participants were instructed to indicate the number of

target stimuli that were presented during the preceding trial. At the beginning of each block, target stimuli were identified as either those appearing at a defined location or colour, counterbalanced across the session. EEG data from blocks in which the target was defined by spatial location were included in micro and meso linear discriminant analyses; all data were included in the sequential dependency forward encoding analysis.

The EEG recordings were digitised at 1024 Hz sampling rate with a 24-bit A/D conversion. The 64 active scalp Ag/AgCl electrodes were arranged according to the international standard 10–20 system for electrode placement(46) using a nylon head cap and with an online reference of FCz. Offline EEG pre-processing was performed using EEGLAB v2021.1(47). The data were initially subjected to a 0.1 Hz highpass filter to remove slow baseline drifts and a 45 Hz lowpass filter to remove high-frequency noise/artifacts before being downsampled to 512 Hz. Data were then re-referenced to the common average before being epoched into segments around each stimulus (-0.125 s to 0.5 s from the stimulus onset). We only included the parietal, parietal-occipital, and occipital sensors in the analyses to *i*) reduce the influence of signals produced by eye movements, blinks, and non-sensory cortices, *ii*) for consistency with similar previous decoding studies (17, 48, 49), and *iii*) to improve decoding accuracy by restricting sensors to those that carried spatial position information (**Supplementary Fig. 1a**).

Neural Decoding. For micro and meso analyses, EEG recordings (epochs) were grouped according to which side of the task-related or unrelated reference plane they were presented. As the task in the EEG experiment was to detect stimuli presented at a specific location, rather than perform a binary judgement (e.g., left or right of fixation), we constructed task boundaries based on the spatial coordinates that were indicative to the target detection task. Thus, the task-related reference plane was defined by the line bisecting the fixation point at an angle orthogonal to the target location, because this plane was most informative of whether a stimulus was a target. By contrast, the task-unrelated plane was the line orthogonal to the task-related line, as this plane was uninformative of whether a stimulus was a target. Ten-fold cross-validation linear discriminant analysis was performed with the MATLAB *classify* function (discriminant function, diaglinear) to calculate the two-way classification accuracy separately at

649 each time point and reference plane. Classification accuracy was then separately
650 assessed for repeat and alternate trials (micro analysis) and the eight pairs of five-
651 event sequences (meso analysis).

652 As shown in **Supplementary Figure 2**, we found that there were differences in
653 classification accuracy for repeat and alternate stimuli in the EEG data, even when
654 stimulus labels were shuffled. This is likely due to temporal autocorrelations within the
655 EEG data that are unrelated to the decoded stimulus dimension. This signal causes
656 the decoder to classify temporally proximal stimuli as the same class, leading to a bias
657 towards repeat classification. For example, in general, the EEG signal during trial one
658 will be more similar to that during trial two than during trial ten, because of low
659 frequency trends in the recordings. If the decoder has been trained to classify the
660 signal associated with trial one as a leftward stimulus, then it will be more likely to
661 classify trial two as a leftward stimulus too. These autocorrelations are unrelated to
662 stimulus features; thus, to isolate the influence of stimulus-specific temporal context,
663 we subtracted the accuracy produced by shuffling the stimulus labels from the
664 unshuffled accuracy. As a further test of this explanation, we performed the same
665 classification analysis on the data after applying a high-pass filter of 0.7 Hz.

666 For serial dependency analyses, we used an inverted modelling approach to
667 reconstruct either the location or Δ location (angular distance from previous stimulus)
668 of the stimuli (50); note, the results of Δ location analyses are shown in
669 **Supplementary Figure 1**. A theoretical (forward) model was nominated that
670 described the measured activity in the EEG sensors given the location/Δ location of
671 the presented stimulus. The forward model was then used to obtain the inverse model
672 that described the transformation from EEG sensor activity to stimulus location/Δ
673 location. The forward and inverse models were obtained using a ten-fold cross-
674 validation approach.

675 Similar to previous work (26, 51, 52), the forward model comprised five
676 hypothetical channels, with evenly distributed idealized location/Δ location preferences
677 between 0° and 360°. Each channel consisted of a half-wave rectified sinusoid raised
678 to the fifth power. The channels were arranged such that a tuning curve of any
679 location/Δ location preference could be expressed as a weighted sum of the five

channels. The observed EEG activity for each presentation could be described by the following linear model:

$$\mathbf{B} = \mathbf{WC} + \mathbf{E} \quad (1)$$

where $\mathbf{B}$ indicates the (*m* sensors × *n* presentations) EEG data, $\mathbf{W}$ is a weight matrix (*m* sensors × 5 channels) that describes the transformation from EEG activity to stimulus location/Δ location, $\mathbf{C}$ denotes the hypothesized channel activities (5 channels × *n* presentations), and $\mathbf{E}$ indicates the residual errors.

To compute the inverse model, we estimated the weights that, when applied to the data, would reconstruct the underlying channel activities with the least error. In line with previous magnetencephalography work (53, 54), when computing the inverse model, we deviated from the forward model proposed by Brouwer and Heeger (2009) (51) by taking the noise covariance into account to optimize it for EEG data, given the high correlations between neighbouring sensors. We then estimated the weights that, when applied to the data, would reconstruct the underlying channel activities with the least error. Specifically, $\mathbf{B}$ and $\mathbf{C}$ were demeaned such that their average over presentations equalled zero for each sensor and channel, respectively. The inverse model was then estimated using a subset of data selected through cross-fold validation. The hypothetical responses of each of the five channels were calculated from the training data, resulting in the response row vector $\mathbf{c}_{train,i}$ of length n_{train} presentations for each channel i. The weights on the sensors $\mathbf{w}_i$ were then obtained through least squares estimation for each channel:

$$\mathbf{w}_i = \boldsymbol{B}_{train}\mathbf{c}_{train,i}^{\mathrm{T}}\left(\mathbf{c}_{\text{train,i}}\mathbf{c}_{train,i}^{\mathrm{T}}\right)^{-1} \quad (2)$$

where $\boldsymbol{B}_{train}$ indicates the (*m* sensors × n_{train} presentations) training EEG data. Subsequently, the optimal spatial filter $\mathbf{v}_i$ to recover the activity of the ith channel was obtained as follows (54):

$$\mathbf{v}_i = \frac{\widetilde{\sum}_i^{-1}\mathbf{w}_i}{\mathbf{w}_i^{\mathrm{T}}\widetilde{\sum}_i^{-1}\mathbf{w}_i} \quad (3)$$

where $\widetilde{\sum}_i$ is the regularized covariance matrix for channel i. Incorporating the noise covariance in the filter estimation leads to the suppression of noise that arises from correlations between sensors. The noise covariance was estimated as follows:

$$\widehat{\sum}_i = \frac{1}{n_{\text{train}} - 1}\boldsymbol{\varepsilon}_i\boldsymbol{\varepsilon}_i^{\mathrm{T}} \quad (4)$$

$$\boldsymbol{\varepsilon}_i = \mathbf{B}_{train} - \mathbf{w}_i \mathbf{c}_{train,i} \quad (5)$$

where n_{train} is the number of training presentations. For optimal noise suppression, we improved this estimation by means of regularization by shrinkage using the analytically determined optimal shrinkage parameter (54), yielding the regularized covariance matrix $\widetilde{\sum}_i$.

For each presentation, we decoded location and Δ location by converting the channel responses to polar form:

$$z = \mathbf{c} \cdot e^{2i\boldsymbol{\varphi}} \quad (6)$$

and calculating the estimated angle:

$$\hat{\theta} = \frac{\arg(z)}{2} \quad (7)$$

where $\mathbf{c}$ is a vector of channel responses and $\boldsymbol{\varphi}$ is the vector of angles at which the channels peak. Decoding accuracy, which represents the similarity of the decoded location/colour to the presented location and Δ location (53), was expressed by projecting the mean resultant (presentations averaged across 12 evenly distributed Δ location bins) of the difference between decoded and arc location onto a vector with 0°:

$$\hat{r}_\theta = \mathrm{Re}[\bar{R}], \quad \bar{R} = \frac{1}{n}\sum_{j=1}^{n} \exp\left(\mathrm{i}\left(\hat{\theta}_j - \theta\right)\right) \quad (8)$$

Precision was estimated by calculating the angular deviation (55) of the decoded orientations within each orientation bin:

$$\hat{\sigma}_\theta = \sqrt{2(1 - |\bar{R}|)} \quad (9)$$

and normalized, such that values ranged from 0 to 1, where 0 indicates a uniform distribution of decoded orientations across all orientations (i.e., chance-level decoding) and 1 represents perfect consensus among decoded orientations:

$$\hat{p}_\theta = 1 - \frac{2\hat{\sigma}_\theta}{\sqrt{2}} \quad (10)$$

Bias was estimated by computing the circular mean of angular difference between the decoded and presented orientation:

$$\hat{b}_\theta = \arg(\bar{R}) \quad (11)$$

As shown in **Supplementary Figure 3**, we found the same general temporal dependencies in the decoding accuracy computed using inverted encoding that were found using linear discriminant classification. However, as a baseline correction would not have been appropriate or effective for the parameters decoded with this approach, we instead used a high-pass filter of 0.7 Hz to remove the confound, while being cautious about interpreting the timing of effects produced by this analysis due to the temporal smear introduced by the filter.

Statistical analyses. Statistical analyses were performed in MATLAB v2020a and CircStat Toolbox v1.12.0.0 (56). Prior to statistical testing of behavioural estimates, within-participant average values of response time, task accuracy, and precision estimates >1.5 times the interquartile range of the group distribution were removed. Non-parametric inferential tests (Wilcoxon signed rank test (57) and Friedman's ANOVA(58)) were used to assess the significance of paired differences and main effects. For Wilcoxon signed rank tests, the rank-biserial correlation (r) was calculated as an estimate of effect size, where 0.1, 0.3, and 0.5 indicate small, medium, and large effects, respectively (59). For Friedman's ANONA tests, Kendal's W was calculated as an estimate of effect size, where 0.1, 0.3, and 0.5 indicate small, medium, and large effects, respectively (60). Levene's test of homogeneity was used to compare the difference in variance between conditions (61). For pupillometry and linear discriminant analyses, one-dimensional cluster correction was applied to remove spurious significant differences (62). For inverted modelling analyses of location and Δ location as a function of Δ location and time, a two-dimensional circular-linear cluster correction was applied. First, at each Δ location and/or time point, the effect size of the dependent variable (e.g., decoding accuracy) was calculated. Next, we calculated the summed value of these statistics (separately for positive and negative values) within contiguous featural and/or temporal clusters of significant values. We then simulated the null distribution of the maximum summed cluster values using permutation (n=5000) of the sign or condition labels, for single and paired t-test comparisons, respectively, from which we derived the 95% percentile threshold value. Clusters identified in the data with a summed effect-size value less than the threshold were considered spurious and removed. Prior to cluster analysis, we smoothed the

decoding accuracy estimates in the inverted modelling analyses along the feature dimension using a uniform kernel (size, 4).

Data and Code Availability. The data and analysis code generated in this study have been deposited in the following OSF database: https://osf.io/9qfdk/

REFERENCES

1. D. M. Wolpert, J. R. Flanagan, Motor prediction. *Current Biology* **11**, R729–R732 (2001).

2. H. B. Barlow, "Possible Principles Underlying the Transformations of Sensory Messages" in *Sensory Communication*, W. A. Rosenblith, Ed. (The MIT Press, 1961), pp. 216–234.

3. K. Friston, A theory of cortical responses. *Philosophical Transactions of the Royal Society B: Biological Sciences* **360**, 815–836 (2005).

4. R. P. N. Rao, D. H. Ballard, Predictive coding in the visual cortex: a functional interpretation of some extra-classical receptive-field effects. *Nat Neurosci* **2**, 79–87 (1999).

5. G. M. Cicchini, G. Anobile, D. C. Burr, Compressive mapping of number to space reflects dynamic encoding mechanisms, not static logarithmic transform. *Proceedings of the National Academy of Sciences* **111**, 7867–7872 (2014).

6. G. M. Cicchini, K. Mikellidou, D. C. Burr, Serial Dependence in Perception. *Annual Review of Psychology* **75**, 129–154 (2024).

7. J. Fischer, D. Whitney, Serial dependence in visual perception. *Nat Neurosci* **17**, 738–743 (2014).

8. N. K. Squires, K. C. Squires, S. A. Hillyard, Two varieties of long-latency positive waves evoked by unpredictable auditory stimuli in man. *Electroencephalography and Clinical Neurophysiology* **38**, 387–401 (1975).

9. N. H. Kirby, Sequential effects in two-choice reaction time: Automatic facilitation or subjective expectancy? *Journal of Experimental Psychology: Human Perception and Performance* **2**, 567–577 (1976).

10. R. J. Remington, Analysis of sequential effects on choice reaction times. *Journal of Experimental Psychology* **82**, 250 (1969).

11. A. Schapiro, N. Turk-Browne, "Statistical Learning" in *Brain Mapping*, (Elsevier, 2015), pp. 501–506.

12. E. P. Simoncelli, B. A. Olshausen, Natural Image Statistics and Neural Representation. *Annu. Rev. Neurosci.* **24**, 1193–1216 (2001).

13. P. Kok, J. F. M. Jehee, F. P. de Lange, Less Is More: Expectation Sharpens Representations in the Primary Visual Cortex. *Neuron* **75**, 265–270 (2012).

14. F. P. de Lange, M. Heilbron, P. Kok, How Do Expectations Shape Perception? *Trends in Cognitive Sciences* **22**, 764–779 (2018).

15. D. Richter, M. Heilbron, F. P. de Lange, Dampened sensory representations for expected input across the ventral visual stream. *Oxford Open Neuroscience* **1**, kvac013 (2022).

16. P. Bertelson, Sequential redundancy and speed in a serial two-choice responding task. *Quarterly Journal of Experimental Psychology* **13**, 90–102 (1961).

17. R. Rideaux, Task-related modulation of event-related potentials does not reflect changes to sensory representations. *Imaging Neuroscience* **2**, 1–13 (2024).

18. G. M. Cicchini, K. Mikellidou, D. C. Burr, The functional role of serial dependence. *Proceedings of the Royal Society B: Biological Sciences* **285**, 20181722 (2018).

19. N. Stewart, Absolute identification is relative: A reply to Brown, Marley, and Lacouture (2007). *Psychological Review* **114**, 533–538 (2007).

20. M. Luo, H. Zhang, F. Fang, H. Luo, Reactivation of previous decisions repulsively biases sensory encoding but attractively biases decision-making. *PLOS Biology* **23**, e3003150 (2025).

21. T. C. Sheehan, J. T. Serences, Attractive serial dependence overcomes repulsive neuronal adaptation. *PLOS Biology* **20**, e3001711 (2022).

22. C. Fischer, J. Kaiser, C. Bledowski, A direct neural signature of serial dependence in working memory. [Preprint] (2024). Available at: https://www.biorxiv.org/content/10.1101/2024.05.13.593912v1 [Accessed 26 September 2024].

23. M. Fritsche, E. Spaak, F. P. de Lange, A Bayesian and efficient observer model explains concurrent attractive and repulsive history biases in visual perception. *eLife* **9**, e55389 (2020).

24. A. Mazancieux, *et al.*, Brainstem fMRI signaling of surprise across different types of deviant stimuli. *Cell Reports* **42**, 113405 (2023).

25. K. Preuschoff, B. ’t Hart, W. Einhauser, Pupil Dilation Signals Surprise: Evidence for Noradrenaline’s Role in Decision Making. *Frontiers in Neuroscience* **5** (2011).

26. R. Rideaux, R. K. West, D. Rangelov, J. B. Mattingley, Distinct early and late neural mechanisms regulate feature-specific sensory adaptation in the human visual system. *Proceedings of the National Academy of Sciences* **120**, e2216192120 (2023).

27. R. Rideaux, *et al.*, Violated predictions enhance the representational fidelity of visual features in perception. [Preprint] (2024). Available at: https://www.biorxiv.org/content/10.1101/2024.03.27.587109v1 [Accessed 31 August 2024].

28. I. Jentzsch, W. Sommer, Functional localization and mechanisms of sequential effects in serial reaction time tasks. *Perception & Psychophysics* **64**, 1169–1188 (2002).

29. J. Gao, K. Wong-Lin, P. Holmes, P. Simen, J. D. Cohen, Sequential Effects in Two-Choice Reaction Time Tasks: Decomposition and Synthesis of Mechanisms. *Neural Computation* **21**, 2407–2436 (2009).

30. F. Galluzzi, A. Benedetto, G. M. Cicchini, D. C. Burr, Visual priming and serial dependence are mediated by separate mechanisms. *Journal of Vision* **22**, 1 (2022).

31. R. Auksztulewicz, K. Friston, Attentional Enhancement of Auditory Mismatch Responses: a DCM/MEG Study. *Cerebral Cortex* **25**, 4273–4283 (2015).

32. C. A. Smout, M. F. Tang, M. I. Garrido, J. B. Mattingley, Attention promotes the neural encoding of prediction errors. *PLOS Biology* **17**, e2006812 (2019).

33. J.-M. Guérit, D. Verougstraete, M. de Tourtchaninoff, D. Debatisse, C. Witdoeckt, ERPs obtained with the auditory oddball paradigm in coma and altered states of consciousness: clinical relationships, prognostic value, and origin of components. *Clinical Neurophysiology* **110**, 1260–1269 (1999).

34. A. Alink, C. M. Schwiedrzik, A. Kohler, W. Singer, L. Muckli, Stimulus Predictability Reduces Responses in Primary Visual Cortex. *J. Neurosci.* **30**, 2960–2966 (2010).

35. H. Den Ouden, P. Kok, F. De Lange, How Prediction Errors Shape Perception, Attention, and Motivation. *Frontiers in Psychology* **3** (2012).

36. T. Meyer, C. R. Olson, Statistical learning of visual transitions in monkey inferotemporal cortex. *Proceedings of the National Academy of Sciences* **108**, 19401–19406 (2011).

37. D. Richter, M. Ekman, F. P. de Lange, Suppressed Sensory Response to Predictable Object Stimuli throughout the Ventral Visual Stream. *J. Neurosci.* **38**, 7452–7461 (2018).

38. A. Todorovic, F. van Ede, E. Maris, F. P. de Lange, Prior Expectation Mediates Neural Adaptation to Repeated Sounds in the Auditory Cortex: An MEG Study. *J. Neurosci.* **31**, 9118–9123 (2011).

39. M. F. Tang, C. A. Smout, E. Arabzadeh, J. B. Mattingley, Prediction error and repetition suppression have distinct effects on neural representations of visual information. *eLife* **7**, e33123 (2018).

40. M. F. Tang, *et al.*, Expectation violations enhance neuronal encoding of sensory information in mouse primary visual cortex. *Nat Commun* **14**, 1196 (2023).

41. Z. Hu, D. M. D. Tran, R. Rideaux, Multimodal evidence challenges the effectiveness of probabilistic cueing for establishing sensory expectations. [Preprint] (2025).

Available at: https://www.biorxiv.org/content/10.1101/2025.03.22.644773v2 [Accessed 22 July 2025].

42. X.-Y. Xie, D. C. Burr, M. C. Morrone, Recent, but not long-term, priors induce behavioral oscillations in peri-saccadic vision. *Commun Psychol* **3**, 41 (2025).

43. D. H. Brainard, The Psychophysics Toolbox. *Spatial Vision* **10**, 433–436 (1997).

44. D. G. Pelli, The VideoToolbox software for visual psychophysics: Transforming numbers into movies. *Spatial Vision* [Preprint] (1997).

45. P. M. Bays, R. F. G. Catalao, M. Husain, The precision of visual working memory is set by allocation of a shared resource. *Journal of Vision* **9**, 7 (2009).

46. R. Oostenveld, P. Praamstra, The five percent electrode system for high-resolution EEG and ERP measurements. *Clinical Neurophysiology* 7 (2001).

47. A. Delorme, S. Makeig, EEGLAB: an open source toolbox for analysis of single-trial EEG dynamics including independent component analysis. *Journal of Neuroscience Methods* **134**, 9–21 (2004).

48. Z. Buhmann, A. K. Robinson, J. B. Mattingley, R. Rideaux, Inverted encoding of neural responses to audiovisual stimuli reveals super-additive multisensory enhancement. *eLife* **13** (2024).

49. R. Rideaux, P. M. Bays, W. J. Harrison, Reply to: "Model mimicry limits conclusions about neural tuning and can mistakenly imply unlikely priors." *Nat Commun* **16**, 6229 (2025).

50. G. J. Brouwer, D. J. Heeger, Cross-orientation suppression in human visual cortex. *Journal of Neurophysiology* **106**, 2108–2119 (2011).

51. G. J. Brouwer, D. J. Heeger, Decoding and reconstructing color from responses in human visual cortex. *Journal of Neuroscience* **29**, 13992–14003 (2009).

52. W. J. Harrison, P. M. Bays, R. Rideaux, Neural tuning instantiates prior expectations in the human visual system. *Nat Commun* **14**, 5320 (2023).

53. P. Kok, P. Mostert, F. P. de Lange, Prior expectations induce prestimulus sensory templates. *Proceedings of the National Academy of Sciences* **114**, 10473–10478 (2017).

54. P. Mostert, P. Kok, F. P. de Lange, Dissociating sensory from decision processes in human perceptual decision making. *Sci Rep* **5**, 18253 (2015).

55. J. H. Zar, *Biostatistical analysis* (Pearson Education India, 1999).

56. P. Berens, CircStat: A MATLAB Toolbox for Circular Statistics. *J. Stat. Soft.* **31** (2009).

57. F. Wilcoxon, “Individual Comparisons by Ranking Methods” in *Breakthroughs in Statistics: Methodology and Distribution*, S. Kotz, N. L. Johnson, Eds. (Springer, 1992), pp. 196–202.

58. M. Friedman, The Use of Ranks to Avoid the Assumption of Normality Implicit in the Analysis of Variance. *Journal of the American Statistical Association* **32**, 675–701 (1937).

59. E. E. Cureton, Rank-Biserial Correlation. *Psychometrika* **21**, 287–290 (1956).

60. M. G. Kendall, *Rank correlation methods* (Griffin, 1948).

61. H. Levene, Robust tests for equality of variances. (1960).

62. C. R. Pernet, M. Latinus, T. E. Nichols, G. A. Rousselet, Cluster-based computational methods for mass univariate analyses of event-related brain potentials/fields: A simulation study. *Journal of Neuroscience Methods* **250**, 85–93 (2015).

eLife

Supplemental Information

The influence of temporal context on visual perception over multiple time scales

Kacie Lee & Reuben Rideaux

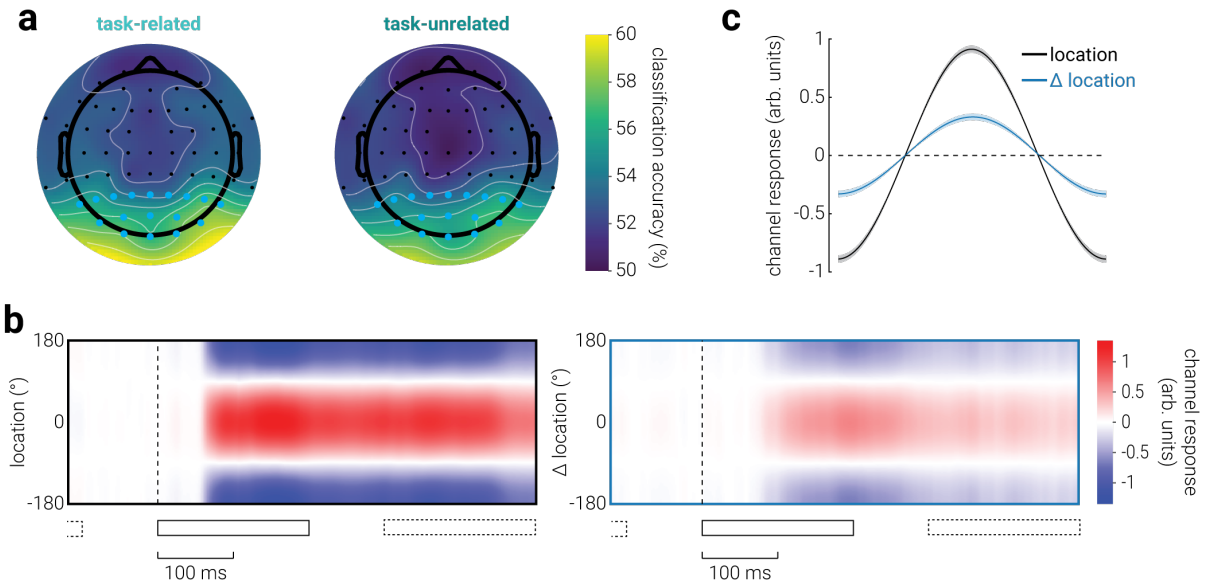

Supplementary Figure 1. Decoding stimulus location and Δ location from EEG recordings. a) Topographic representation of task-related and unrelated stimulus location information produced using linear discriminant analysis to classify stimulus location, separately for each sensor, with time as the multivariate dimension. Blue dots indicate the sensors that were subsequently used in all other EEG analyses. **b**) Channel responses for location and Δ location, produced by computing the dot product between the inverted model channel responses and the forward model, as a function of time. **c**) The average channel response for location and Δ location between 0-500 ms following stimulus onset.

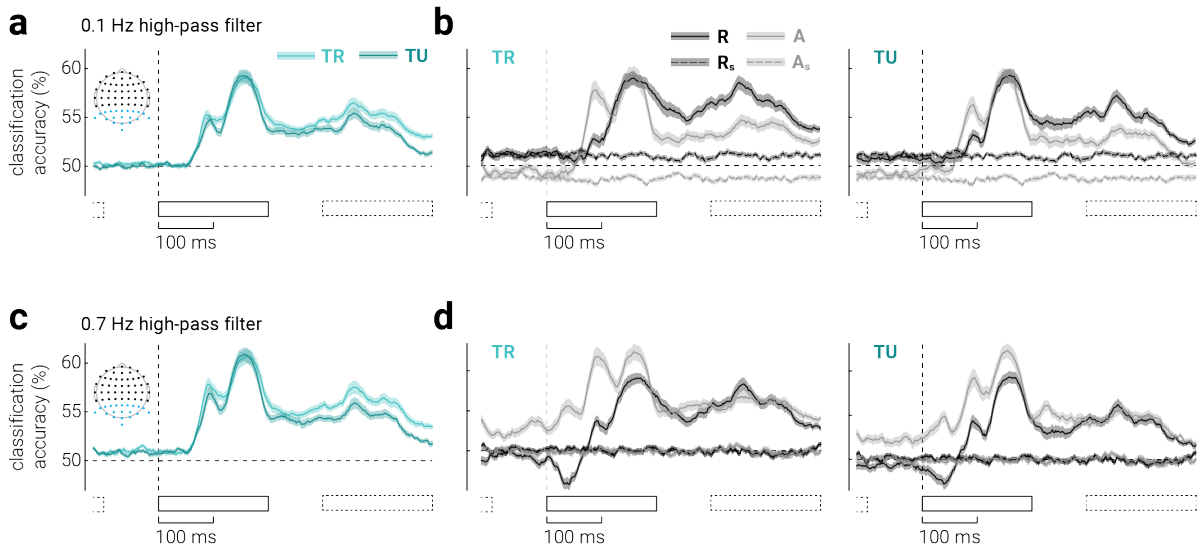

Supplementary Figure 2. Removal of general micro temporal dependencies in EEG responses. We found that there were differences in classification accuracy for repeat and alternate stimuli in the EEG data, even when stimulus labels were shuffled. This is likely due to temporal autocorrelation within the EEG data due to low frequency signal changes that are unrelated to the decoded stimulus dimension. This signal trains the decoder to classify temporally proximal stimuli as the same class, leading to a bias towards repeat classification. For example, in general, the EEG signal during trial one is likely to be more similar to that during trial two than during trial ten, because of low frequency trends in the recordings. If the decoder has been trained to classify the signal associated with trial one as a leftward stimulus, then it will be more likely to classify trial two as a leftward stimulus too. These autocorrelations are unrelated to stimulus features; thus, to isolate the influence of stimulus-specific temporal context, we subtracted the classification accuracy produced by shuffling the stimulus labels from the unshuffled accuracy (as presented in **Figure 2e, f**). We confirmed that using a stricter high-pass filter (0.7 Hz) removes this artifact, as indicated by the equal decoding accuracy between the two shuffled conditions. However, the stricter high-pass filter temporally smears the stimulus-related signal, which introduces other (stimulus-related) artifacts, e.g., above-chance decoding accuracy prior to stimulus presentation, that are larger and more complex, i.e., changing over time. Thus, we opted to use the original high pass filter (0.1 Hz) and apply a baseline correction. **a**) The uncorrected classification accuracy along task related and unrelated planes. Note that these results are the same as the corrected version shown in **Figure 2e**, because the confound is only apparent when accuracy is grouped according to temporal context. **b**) Same as (**a**), but split into repeat and alternate stimuli, along (left) task-related and (right) unrelated planes. Classification accuracy when labels are shuffled is also shown. Inset in (**a**) shows the EEG sensors included in the analysis (blue dots). (**c**, **d**) Same as (**a**, **b**), but on data filtered using a 0.7 Hz high-pass filter. Black rectangles indicate the timing of stimulus presentations (solid: target stimulus, dashed: previous and subsequent stimuli). Shaded regions indicate ±SEM.

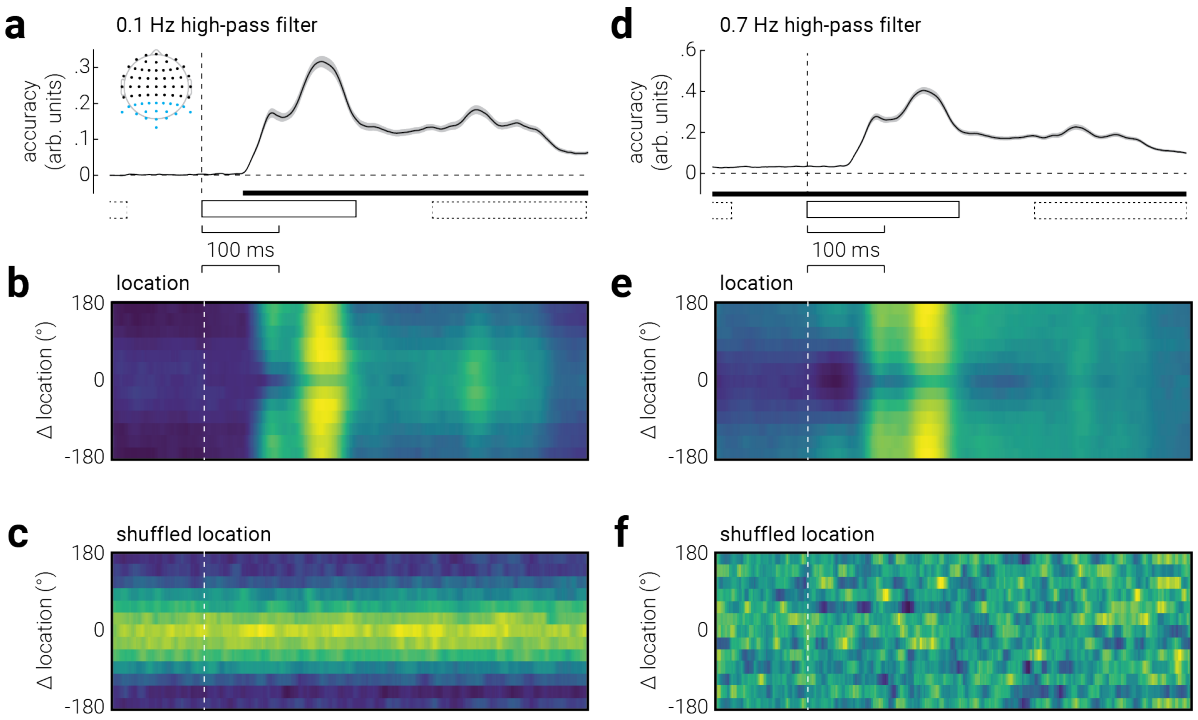

Supplementary Figure 3. Removal of general temporal dependencies in EEG responses for inverted encoding analyses. As described in *Methods - Neural Decoding,* we used inverted encoding modelling of EEG recordings to estimate the decoding accuracy, precision, and bias of stimulus location. Just as in the linear discriminant classification analysis, we also found the influence of general temporal dependencies in the results produced by the inverted encoding analysis. In particular, there was increased decoding accuracy for targets with low Δ location. This was weakly evident in the period prior to stimulus presentation, but clearly visible when the labels were shuffled. These results are mirror those from the classification analysis, albeit in a more continuous space. However, whereas in the classification analysis it was straightforward to perform a baseline correction to remove the influence of general temporal dependency, the more complex nature of the accuracy, precision, and bias parameters over the range of time and Δ location makes this approach less appropriate. For example, the bias in the shuffled condition ranged from -180° to 180°, which when subtracted from the bias in the unshuffled condition would produce an equally spurious outcome, i.e., the equal opposite of this extreme bias. Instead for the inverted encoding analysis, we used the data high-pass filtered at 0.7 Hz. As with the classification analysis, this significantly reduced the influence of general temporal dependencies, as indicated by the results of the shuffled data analysis, but it also temporally smeared the stimulus-related signal, resulting in above chance decoding accuracy prior to stimulus onset. However, we were primarily interested in the pattern of accuracy, precision, and bias as a function of Δ location, and less concerned with the precise temporal dynamics of these changes. Thus, this was the more suitable approach to removing the general temporal dependencies in the inverted encoding analysis and the one that is presented in **Figure 3**. (**a**) Decoding accuracy as a function of time for the EEG data filtered using a 0.1 Hz high-pass filter. Inset shows the EEG sensors included in the analysis (blue dots), and black rectangles indicate the timing of stimulus presentations (solid: target stimulus, dashed: previous and subsequent stimuli). (**b, c**) The same as (**a**), but as a function of time and Δ location for (**b**) the original data and (**c**) data with shuffled labels. (**d-f**) Same as (**a-c**), but for data filtered using a 0.7 Hz high-pass filter. Shaded regions in (**a**, **d**) indicate ±SEM. Horizontal bars in (**a, d**) indicate cluster corrected periods of significance; note, all time points in (**d**) were significantly above chance. Note, the temporal abscissa is vertically aligned across plots (**a-c** & **d-f**).

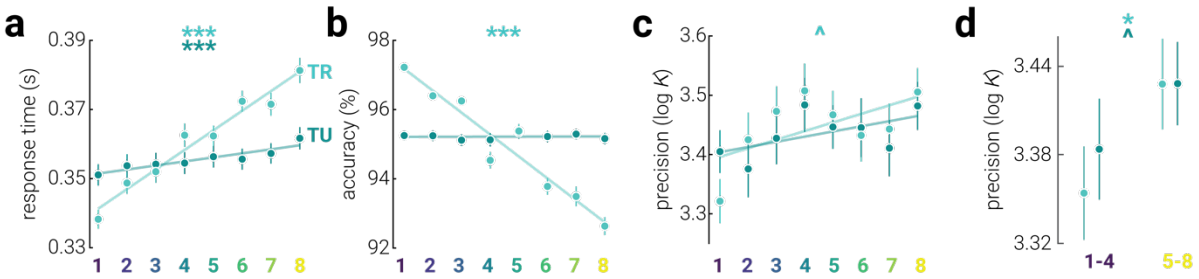

Supplementary Figure 4. Meso-scale temporal context effects in Experiment 2. a) Response time, (**b**) task accuracy, and (**c**) precision as a function of sequence, across task-related and unrelated reference planes. Note, lower numbers on the abscissa are associated with more expected sequences. **d**) Same as (**c**), but pooled across the four most expected (1-4) and unexpected sequences (1-8). Asterisks indicate significant correlations with sequence order (*p<.05, **p<.01, ***p<.001), hats indicate marginal significance (^p<.06). Error bars indicate ±SEM.

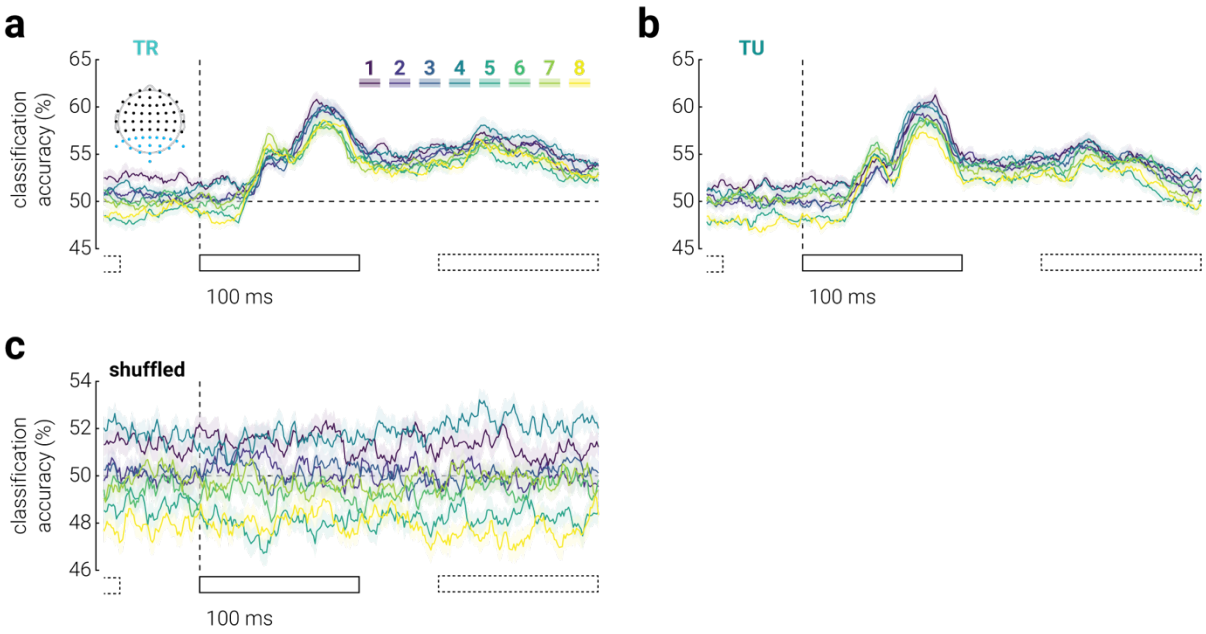

Supplementary Figure 5. Removal of general meso temporal dependencies in EEG responses. To remove any potential general sequential dependences from the meso-scale classification analysis of EEG recordings, we performed the same subtraction method as used in the micro-scale analysis. (**a**) Classification accuracy of stimuli presented on different sides of task-related planes as a function of time, for each of the eight sequences, from re-analysis of previously published EEG data (17). **b**) Same as (**a**), but for the task-unrelated plane. (**c**) Same as (**a**), but with shuffled labels. **Figure 4f, g** shows (**a**, **b**) after removing shuffled accuracy (**c**). Inset in (**a**) shows the EEG sensors included in the analysis (blue dots). Black rectangles indicate the timing of stimulus presentations (solid: target stimulus, dashed: previous and subsequent stimuli). Shaded regions indicate ±SEM.

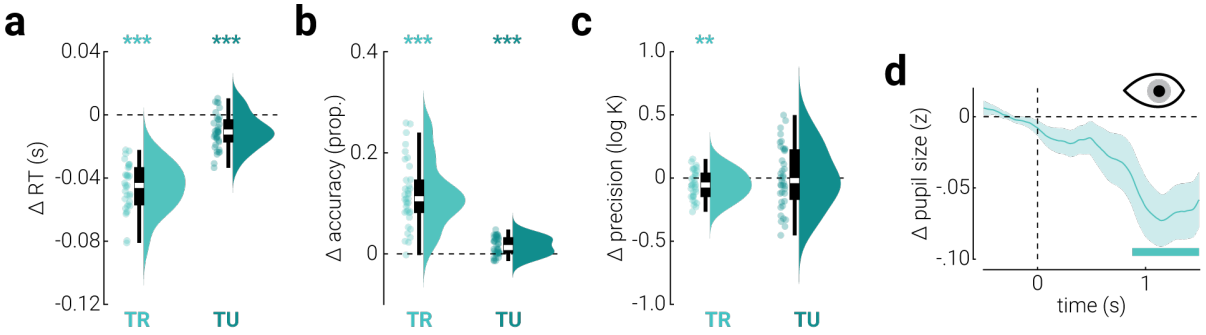

Supplementary Figure 6. Macro-scale temporal context effects in Experiment 3. a-c) The difference (expected – unexpected) in (**a**) response time, (**b**) task accuracy, and (**c**) reproduction precision between expected and unexpected stimuli, along task-related (TR) and unrelated (TU) planes. Asterisks indicate significant differences (**p<.01, ***p<.001). **d**) The difference (expected – unexpected) in pupil size as a function of time from stimulus presentation, along the task-related (TR) plane. Shaded region indicates ±SEM and the horizontal bar indicates a cluster corrected period of significant difference.